PERGAMON

International Journal of Heat and Mass Transfer 43 (2000) 3219–3231

International Journal of HEAT and MASS TRANSFER

www.elsevier.com/locate/ijhmt

Large eddy simulation of indoor airflow with a filtered dynamic subgrid scale model

Wei Zhang, Qingyan Chen*

Building Technology Program, Massachusetts Institute of Technology, 77 Massachusetts Avenue, Cambridge, MA 02139, USA

Received 12 February 1999; received in revised form 10 July 1999

Abstract

Accurate prediction of the distributions of indoor airflow is very important for designing a comfortable and healthy indoor environment. This paper uses a large eddy simulation (LES) program with a filtered dynamic subgrid scale model to calculate natural, forced and mixed convection flows in rooms. The predicted air velocity, air temperature and turbulence distributions agree reasonably well with the corresponding experimental data. The LES has great potential for the simulation of indoor airflow. © 2000 Elsevier Science Ltd. All rights reserved.

Keywords: Large eddy simulation; Subgrid scale model; Filtering technique; Indoor airflow

1. Introduction

To design a comfortable and healthy indoor environment requires information about the distributions of air velocity, air temperature, relative humidity, contaminant concentrations, and turbulent quantities. However, most indoor airflows are complicated, and are driven by pressure gradient and thermal buoyancy. Typical indoor airflow includes natural convection, such as winter heating by a baseboard convector, forced convection, such as free cooling in spring seasons, and mixed convection, such as summer cooling with an air conditioning unit. It is very challenging to predict indoor airflow.

1.1. Approaches available for indoor airflow studies

Two common approaches are available to study indoor airflow: experimental measurements and computer simulation. The experimental approach normally uses a full-scale environmental chamber to simulate an indoor space and to isolate the space from the external world. The requirement of a full-scale chamber is due to scaling problems for non-isothermal flow. The isolation allows for the creation of controllable thermal and fluid boundary conditions. However, the full-scale environmental chamber is expensive, and a measurement may take many months to complete.

The other research approach is to use computational-fluid-dynamics (CFD) to calculate indoor airflow. Considerable success has been achieved by using the CFD for indoor airflow, although there are still some difficulties as reviewed by Chen [1]. The CFD is further divided into three types: direct numerical simulation (DNS), Reynolds averaged Navier–Stokes (RANS) equation modeling, and large eddy simulation (LES).

The DNS solves the highly reliable Navier–Stokes equations without approximations. The method requires a grid resolution as fine as the Kolmogorov microscale. This requires a grid resolution of around

* Corresponding author. Tel.: +1-617-253-7714; fax: +1-617-253-6152.

E-mail address: qchen@mit.edu (Q. Chen).

0017-9310/00/$ - see front matter
PII: S0017-9310(99)00348-8

Nomenclature

$Ar = \frac{\beta g h_{in} \Delta T_0}{U_{in}^2}$	Archimedes number	$\tilde{u}_i$	test filtered velocities
C	dynamic subgrid scale model coefficient	$\boldsymbol{v}$	velocity vector
		W	room depth (forced convection case)
C_S	Smagorinsky model coefficient	x, y, z	three components in Cartesian coordinates
D	room depth (mixed convection case)		
$G(x_i)$	filter function	x_i	Cartesian space coordinate
g	gravitational acceleration	β	thermal expansion coefficient
H	room height	θ	temperature
L	room width	$\bar{\theta}$	grid filtered temperature
Pr	molecular Prandtl number	$\tilde{\theta}$	test filtered temperature
Pr_{SGS}	subgrid scale Prandtl number	ΔT	dimensionless time step
$\bar{P}$	grid filtered pressure	Δt	time step
Ra	Rayleigh number	$\bar{\Delta}$	grid filter size
T	temperature	$\tilde{\Delta}$	test filter size
u_i	velocities	ν	kinematic viscosity
$\bar{u}_i$	grid filtered velocities	$\mathbf{x}$	vector in x direction

10^{13} for airflow in a room. Current supercomputers can have a grid resolution of 10^7. Therefore, the DNS cannot be used to study indoor airflow under a realistic condition.

The RANS solves ensemble-averaged Navier–Stokes equations by using turbulence modeling. The most widely used turbulence model is the standard k–ε model [2]. Chen [3,4] compared five different k–ε models and three Reynolds stress models for the prediction of natural, forced, and mixed convection flows in rooms, as well as an impinging jet flow. The performance of those models is generally poor. One model can perform very well for one type of flow, but very poorly for another type. None of the models tested is universal. Hence, it is very difficult for a designer to select an appropriate turbulence model, since most of the designers do not know very much about turbulence modeling. In addition, many turbulence models, such as the Reynolds stress models, can be mathematically complex and numerically unstable. Furthermore, they cannot calculate the power spectrum of airflow, that is a very interesting thermal comfort parameter.

The LES developed in 1963 by Smagorinsky [6] for meteorological applications and in 1970s by Deardorff [5] for industrial applications assumes that turbulent motion could be separated into large-eddies and small-eddies. The separation between the two does not have a significant effect on the evolution of the large-eddies. The LES solves the large eddy motion by a set of filtered equations governing the three-dimensional, time dependant motions. Turbulent transport approximations are used for small-eddies, and the small-eddies are modeled independently from the flow geometry. The success of the LES stems from the fact that the main contribution to turbulent transport comes from the large-eddy motion. Since the LES solves time-dependent flow, it can provide detailed information on turbulence, such as three-dimensional instantaneous velocity. The LES can also provide the information about power spectrum of airflow.

1.2. Subgrid scale models for large-eddy simulation

The key to successfully predicting indoor airflow by the LES is to accurately represent the unresolved subgrid-scale (SGS) motion. The most widely used SGS model is the Smagorinsky model (SM) [6]. However, the model has some notable drawbacks including (a) the requirement of a model coefficient C that is flow dependent; (b) incorrect prediction of the asymptotic behavior near a wall, (c) no permission of SGS energy backscatter to the resolved scales, and (d) problem with transition of turbulence flow prediction. Examples of the SM performance for different types of flow can be found [5].

Germano et al. [7] and Lilly [8] proposed a dynamic subgrid scale model (DSM) to solve the problems associated with the SM by computing directly the model coefficient with the information from the resolved scales. In other words, the model coefficient can be obtained as a function of flow domain and time. This model can also predict correctly the asymptotic behavior near a wall, and permits energy backscatter from small scales to large scales. The DSM has been successfully used in some simple flows, such as channel flow [7], but the DSM still needs improvements for complex flows. For example, the model coefficient

computed has a volatile fluctuation, as found in jet flow [9] and flow around a square cylinder [10]. Although averaging the model coefficient over the homogeneous direction can often reduce the fluctuation [7], it is difficult, if not impossible, to find the homogeneous direction in a complex indoor airflow.

Another method is to average the coefficient locally, such as by volume averaging [11]. The method can effectively reduce the fluctuation for low Reynolds number cavity flow, but our experience shows that the method does not work for high Reynolds number indoor airflow.

Ghosal et al. [12] proposed a fully localized model based on a constrained variation approach. The approach solves Fredholm's integral equation of a second kind and is very complicated. There is no evidence that the model will perform much better for complex indoor airflow.

Another approach by Meneveau et al. [13] used a Lagrangian dynamic model. This model is suitable for inhomogeneous flows and the results are encouraging. However, it has introduced an additional parameter, the Lagrangian averaging time, which needs to be prescribed. Additional tests are required to establish how to calculate this parameter [14].

1.3. Large eddy simulation of indoor airflow

The LES has been used to study indoor airflow recently. Early work is for force convection [15,16] and mixed convection [17] in a room. The computed results show that the LES is very powerful and encouraging. One of the investigations [16] used SM for sub-grid scale motion. The studies showed that the computed velocity depends strongly on the model coefficient. The coefficient has to be tuned in order to obtain the best fit with the corresponding experimental data. If the LES is used as a design tool and no experimental data is available beforehand, there is no way to tune the model coefficient. Davidson and Nielson [15] used the DSM and a very fine numerical grid. However, their computed results deviated from the experimental data. The discrepancies may be attributed to the average of the model coefficient for the DSM in span-wise direction that may not be homogeneous. Murakami et al. [17] also averaged the model coefficient for the DSM in a homogeneous direction. The averaging method cannot be applied to indoor airflow without a homogeneous direction.

Therefore, it is necessary to solve the problem of how to average the coefficient in the DSM for indoor airflow without a homogeneous direction. Our investigation proposes a new simplified and localized coefficient for the DSM with a filtering technique, referred to as filtered dynamic subgrid scale model (FDSM). The FDSM is demonstrated by applying it to study forced, natural, and mixed convection flows indoors. The corresponding experimental data available from the literature and the computed results with the SM will be used for comparison. The aim of the study is to examine if the FDSM can correctly predict indoor airflow.

2. Governing equations and models

2.1. Filter function and governing equations

The LES separates small-eddies from large-eddies with a filter in order to make the turbulence flow solvable. For one-dimensional flow, the filtered velocity is:

$$\overline{u_i} = \int G(x, x')u_i(x')\,\mathrm{d}x' \tag{1}$$

where $G(x, x')$ is a filter function. The filter function is large only when $x - x'$ is less than the filter width, a length scale over which averaging is performed. The flow eddies larger than the filter width are "large-eddies" and smaller than the width are "small-eddies".

In the physical spaces, usually a box filter is used, i.e.:

$$G(x_i) = \begin{cases} \dfrac{1}{\Delta_i} & \left(|x_i| \le \dfrac{\Delta_i}{2}\right) \\ 0 & \left(|x_i| > \dfrac{\Delta_i}{2}\right) \end{cases}, \tag{2}$$

With the finite volume method, it seems natural to define the filter width, Δ_i, as an average over a grid volume. For a three-dimensional flow,

$$\Delta = \left(\prod_{i=1}^{3}\Delta x_i\right)^{1/3}.$$

Applying the filter to the Navier–Stokes equations for an incompressible flow, the equations become:

$$\frac{\partial \overline{u_i}}{\partial t} + \frac{\partial}{\partial x_j}\left(\overline{u_i}\cdot\overline{u_j}\right) = -\frac{1}{\rho}\frac{\partial \bar{P}}{\partial x_i} + \nu\frac{\partial^2 \overline{u_i}}{\partial x_i \partial x_j} - \frac{\partial \tau_{ij}}{\partial x_j} + g_j\beta\left(\bar{\theta} - \theta_0\right)\delta_{ij} \tag{3}$$

where the anisotropic part of the subgrid Reynolds stresses are

$$\tau_{ij} = \overline{u_i u_j} - \overline{u_i}\cdot\overline{u_j} \tag{4}$$

The filtered continuity equation is:

$$\frac{\partial \overline{u_i}}{\partial x_i} = 0 \tag{5}$$

and the filtered energy equation is:

$$\frac{\partial \bar{\theta}}{\partial t} + \frac{\partial \overline{u_j}\bar{\theta}}{\partial x_j} = \frac{\partial}{\partial x_j}\left(\frac{\nu}{Pr}\frac{\partial \bar{\theta}}{\partial x_j}\right) - \frac{\partial h_j}{\partial x_j} \tag{6}$$

where the subgrid heat fluxes are

$$h_j = \overline{u_j\theta} - \overline{u_j}\bar{\theta} \tag{7}$$

The subgrid Reynolds stresses and heat fluxes are unknown and need to be modeled.

2.2. Smagorinsky model (SM)

The simplest subgrid model was the one proposed by Smagorinsky [6]:

$$\tau_{ij} = -2\nu_{\mathrm{SGS}}\overline{S_{ij}} \tag{8}$$

where

$$\nu_{\mathrm{SGS}} = \left(C_{\mathrm{S}}\bar{\Delta}\right)^2\left(2\overline{S_{ij}}\cdot\overline{S_{ij}}\right)^{1/2}, \qquad \overline{S_{ij}} = \frac{1}{2}\left(\frac{\partial \overline{u_i}}{\partial x_j} + \frac{\partial \overline{u_j}}{\partial x_i}\right) \tag{9}$$

and

$$h_j = \alpha_{\mathrm{SGS}}\frac{\partial \bar{\theta}}{\partial x_j}, \text{ and } \alpha_{\mathrm{SGS}} = \frac{\nu_{\mathrm{SGS}}}{Pr_{\mathrm{SGS}}} \tag{10}$$

where, $|\bar{S}| = (2\overline{S_{ij}}\cdot\overline{S_{ij}})^{1/2}$, $C = C_{\mathrm{S}}^2$, $C_{\mathrm{S}} = 0.1$–0.25 [17], and $Pr_{\mathrm{SGS}} = 0.5$ [17].

In near wall region, the turbulence becomes insignificant and the above subgrid scale model does not work, therefore, the Van Driest damping function is used:

$$\Delta = \left(1 - \exp\left(-y^+/25\right)\right)(\Delta x\Delta y\Delta z)^{1/3} \tag{11}$$

where y^+ is the dimensionless distance from the wall.

2.3. Dynamic subgrid scale model (DSM)

The model coefficient C in SM depends on flow type. It even varies in different parts of a flow domain. Therefore, the model coefficient is not an ad-hoc constant. With a constant C, the predicted results deviate very much from the DNS data as shown in [7]. Hence, the constant C should be expressed as a function of time and flow type. Germano [7] and Lilly [8] proposed a dynamic subgrid scale model (DSM). The DSM calculates the C by relating the subgrid scale Reynolds stresses to two different sizes of filters. Since the Reynolds stresses vary with time and location, the C is therefore a function of time and location.

The DSM uses an explicit test filter, $\tilde{G}$, with a filter width of $\tilde{\Delta}(\tilde{\Delta} > \bar{\Delta})$ to determine the turbulent stress on the $\tilde{G}$ filter:

$$T_{ij} = \widetilde{\overline{u_i u_j}} - \tilde{\bar{u}}_i\tilde{\bar{u}}_j \tag{12}$$

The first term on the right-hand side of the equation cannot be determined directly, as that in Eq. (4). However, the term can be eliminated by substituting Eq. (12) from the Eq. (4) with a test filter:

$$T_{ij} - \tilde{\tau}_{ij} = L_{ij} \tag{13}$$

where

$$L_{ij} = \widetilde{\bar{u}_i\bar{u}_j} - \tilde{\bar{u}}_i\tilde{\bar{u}}_j \tag{14}$$

The resolved turbulent stresses in Eq. (14), L_{ij}, can be calculated explicitly. With the definition of Smagorinsky model, the stresses of the test filter, T_{ij}, and that of the grid filter, τ_{ij}, the model coefficient can be calculate by Eq. (12) as

$$C = \frac{\langle L_{ij}M_{ij}\rangle}{\langle M_{ij}M_{ij}\rangle} \tag{15}$$

where

$$L_{ij} = \bar{u}_i\bar{u}_j - \tilde{\bar{u}}_i\tilde{\bar{u}}_j \tag{16}$$

and

$$M_{ij} = \left(2\tilde{\bar{\Delta}}^2|\tilde{\bar{S}}|\tilde{\bar{S}}_{ij} - 2\widetilde{\bar{\Delta}^2|\bar{S}|\bar{S}_{ij}}\right) \tag{17}$$

with

$$\tilde{\bar{S}}_{ij} = \frac{1}{2}\left(\frac{\partial \tilde{\bar{u}}_i}{\partial x_j} + \frac{\partial \tilde{\bar{u}}_j}{\partial x_i}\right), \quad |\tilde{\bar{S}}| = \sqrt{2\tilde{\bar{S}}_{ij}\tilde{\bar{S}}_{ij}} \tag{18}$$

The above equations use a second filter, the test filter ($\tilde{}$), introduced by Germano [7]. The test filter width $\tilde{\Delta}$ is larger than the grid filter width $\bar{\Delta}(\tilde{\bar{\Delta}} = 2.0\bar{\Delta})$ as suggested by Germano [7].

The braces $\langle\,\rangle$ denote an average over the homogeneous directions that can stabilize calculation. Since the C is not a constant, the model is referred to as a DSM.

Similarly, Lilly [8] proposed to determine the Prandtl number of the dynamic subgrid scale by:

$$\frac{1}{Pr_{\mathrm{SGS}}} = \frac{1}{C}\frac{P_jR_j}{R_j^2} \tag{19}$$

where

$$P_j = \widetilde{\bar{u}_j\bar{\theta}} - \tilde{\bar{u}}_j\tilde{\bar{\theta}}, \tag{20}$$

and

$$R_j = 2\tilde{\bar{\Delta}}^2|\tilde{\bar{S}}|\frac{\partial\tilde{\bar{\theta}}}{\partial x_j} - \widetilde{2\bar{\Delta}^2|\bar{S}|\frac{\partial\bar{\theta}}{\partial x_j}} \tag{21}$$

This model has successfully predicted simple channel flow. The averaged formulation effectively stabilizes at least one homogeneous direction.

2.4. Filtered dynamic subgrid scale model (FDSM)

We found a large fluctuation of the DSM coefficient in inhomogeneous indoor airflow. This may be attributed to the high Reynolds number in the indoor airflow, as the coefficient depends on the turbulent scale and flow type. Unfortunately, it is impossible to find a homogeneous flow direction to make a mean. Without a mean, the large fluctuation makes the computation unstable and difficult to converge.

In order to apply the DSM to such a flow, we propose a filtering approach, since the filtering technique cannot only reduce the fluctuation but also reserve local characteristics of the model coefficient. The approach assumes a statistical homogeneity in every filtered grid space. The next section discusses the filtering technique.

The DSM calculates the model coefficient by relating the subgrid scale Reynolds stresses to two different sizes of filters. The error associated with a model τ_{ij}^{model} is given by

$$e_{ij} = L_{ij} - \left(T_{ij}^{\text{model}} - \tilde{\tau}_{ij}^{\text{model}}\right) \tag{22}$$

For the Smagorinsky model, the error equation can be written by [12]

$$e_{ij} = L_{ij} - CM_{ij} \tag{23}$$

The present investigation uses the least-square approach to obtain the localized coefficient, the C in Eq. (23), as suggested by Lilly [8]. At any given point in a space, $\boldsymbol{x}$, the e_{ij} is a function of the C but depends on the $\boldsymbol{x}$. In order to obtain an optimal C, the e_{ij} must be integrated over the entire flow domain. The integration is in consistency with the least-square approach that requires the optimization over the entire flow domain. Since the square of the residual, $e_{ij}e_{ij}$, may have a locally violent change, the $e_{ij}e_{ij}$ should be integrated in the entire flow domain with a smooth function. Thus, the integrated square of the error function, $E_{ij}(C)$, is

$$E_{ij}(C) = \int G_f(\boldsymbol{x}, \boldsymbol{x}')e_{ij}(\boldsymbol{x}')e_{ij}(\boldsymbol{x}')\,\mathrm{d}\boldsymbol{x}' \tag{24}$$

Substitute Eq. (23) into Eq. (24) to yield:

$$E_{ij}(C) = \int G_f(\boldsymbol{x}, \boldsymbol{x}')\left(L_{ij} - CM_{ij}\right)^2\,\mathrm{d}\boldsymbol{x}' \tag{25}$$

Since the least square condition for the Eq. (25) is $\frac{\partial E_{ij}(C)}{\partial C} = 0$, then the optimal model coefficient C is obtained as:

$$C = \frac{\int G_f(\boldsymbol{x}, \boldsymbol{x}')L_{ij}M_{ij}\,\mathrm{d}\boldsymbol{x}'}{\int G_f(\boldsymbol{x}, \boldsymbol{x}')M_{ij}M_{ij}\,\mathrm{d}\boldsymbol{x}'} \tag{26}$$

The smooth function $G(\boldsymbol{x}, \boldsymbol{x}')$ should be chosen for the entire flow domain and may depend on the turbulent scales. Although the smooth function can be in many forms, a box filter function (grid filter) may be most convenient. Then

$$C = \frac{\overline{L_{ij}M_{ij}}}{\overline{M_{ij}M_{ij}}} \tag{27}$$

If the model coefficient is filtered with only one grid filter (Eq. (27)), this procedure is very similar to the local volume averaging method. Our calculations show that the filtered coefficient still fluctuates a lot. Therefore, we use a two-time filter (Eq. (28)). Eq. (28) is an ad-hoc approach referred as a filtered dynamic subgrid scale model (FDSM).

$$C = \overline{\left(\frac{\overline{L_{ij}M_{ij}}}{\overline{M_{ij}M_{ij}}}\right)} \tag{28}$$

Eq. (28) is the new model. The filtered model coefficient calculated by Eq. (28) can be negative locally. A negative C indicates a negative eddy viscosity and implies a flow of energy from small scales to the resolved scales or backscatter, according to Piomelli et al. [18]. However, the negative C can also lead to numerical instability. In order to avoid the instability, the present investigation uses $C = \max(0.0, \text{Eq. (28)})$.

Since the Prandtl number of dynamic subgrid scale does not fluctuate very much, the present investigation uses:

$$\frac{1}{Pr_{\text{SGS}}} = \frac{1}{2C}\frac{\overline{P_jR_j}}{\bar{R}_j^2} \tag{29}$$

If $R_j < 10^{-4}$, $R_j = 10^{-4}$ for numerical stability.

3. Numerical procedure

This study uses a finite difference method to solve the spatially filtered Navier–Stokes equations and a staggered mesh with a pressure-smoothing technique. The discretion of the convection terms is a major source of numerical error in LES calculation. Thus, it

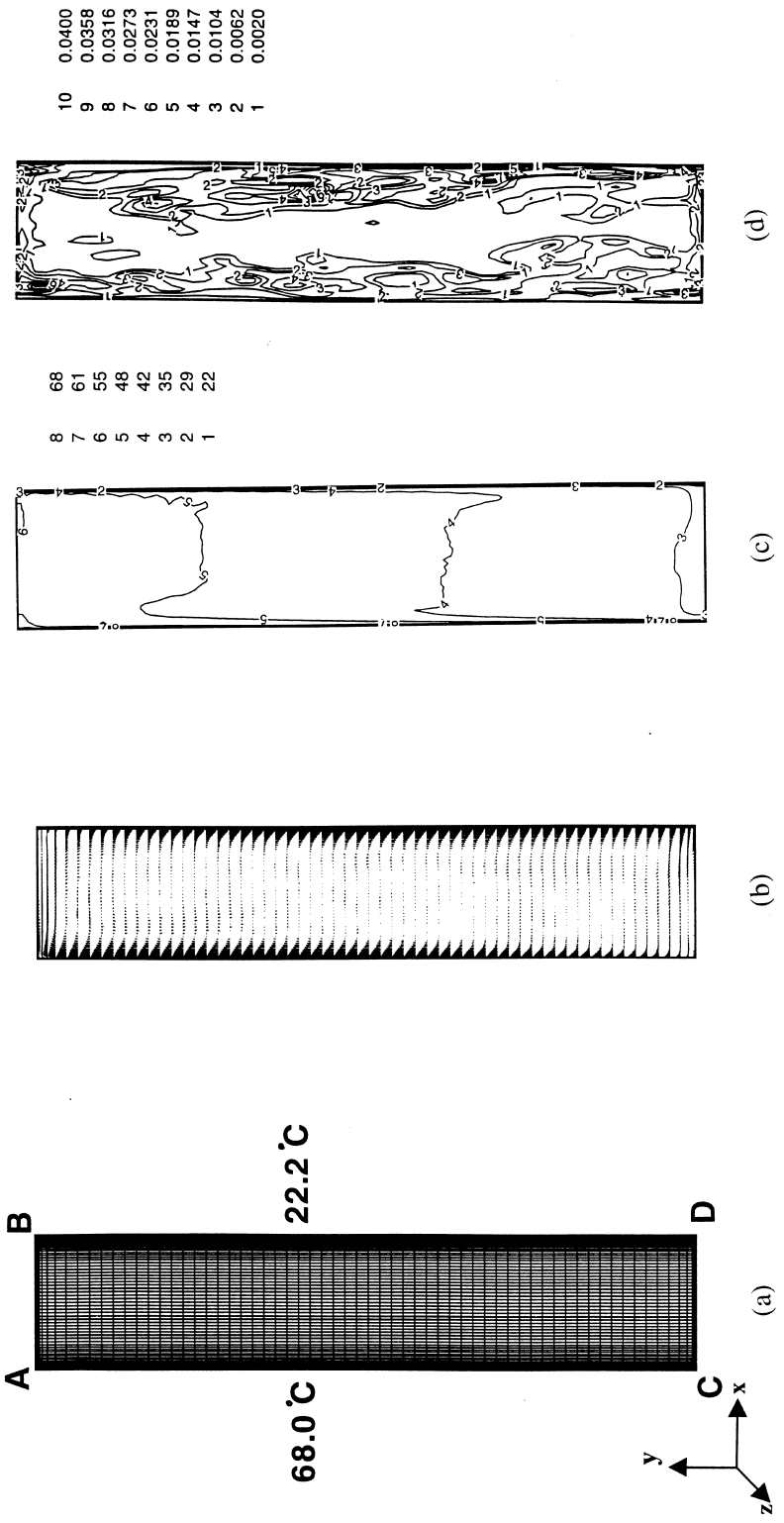

Fig. 1. The predicted results of the natural convection in a cavity with the FDSM at depth = 0.25. (a) The cavity geometry, (b) average air velocity, (c) average air temperature, and (d) instantaneous model coefficient C.

is very important to choose a proper scheme to discretizes the convection terms.

Lower-order numerical schemes, such as the upwind scheme, are very stable. Unfortunately, this scheme generates an unacceptable numerical error that is important for LES simulations. On the other hand, it is well known that higher-order schemes, such as the central differencing scheme, can exhibit oscillation behavior. The central scheme is unstable for numerical solutions. However, the central differencing scheme holds second-order accuracy, and can also satisfy the filter function symmetry law [19]. Furthermore, many researchers have obtained satisfactory results using the second-order central scheme for the convection terms in the LES. Though there are many high-order schemes available, these schemes are not well tested and they may not satisfy the filter function symmetry law.

Therefore, the present study discretizes all spatial terms with the second-order central differencing scheme. A second-order explicit differencing scheme (Explicit Adams–Bashforth Scheme) is used to discretize time. The overall accuracy of the scheme is still second-order. For example, the velocity, $\boldsymbol{v}^*$, is calculated by,

$$\frac{\boldsymbol{v}^* - \boldsymbol{v}^n}{\Delta t} = \frac{3}{2}\{ - \mathrm{grad} \cdot P + (\nu + \nu_{\mathrm{SGS}})\Delta \boldsymbol{v} - (\boldsymbol{v} \cdot \nabla)\boldsymbol{v}\}^n - \frac{1}{2}\{ - \mathrm{grad} \cdot P + (\nu + \nu_{\mathrm{SGS}})\Delta \boldsymbol{v} - (\boldsymbol{v} \cdot \nabla)\boldsymbol{v}\}^{n-1} \quad (30)$$

with the following Poisson equation for the scalar potential φ:

$$\nabla^2 \varphi = -\mathrm{div} \cdot \boldsymbol{v}^* \quad (31)$$

and,

$$\boldsymbol{v}^{n+1} = \boldsymbol{v}^n + \mathrm{grad} \cdot \varphi \quad (32)$$

$$P^{n+1} = P^n - \frac{1}{\Delta t}\varphi \quad (33)$$

The $\boldsymbol{v}^{n+1}$ can be explicitly solved from the above equations. The solving procedure is called simplified maker and cell (SMAC) method [20]. The solution of the Poisson equation is by the strong-implicit procedure (SIP) [21].

4. Applications to indoor airflow studies

This paper applies the FDSM model to indoor airflow simulations. Indoor airflow can be divided into

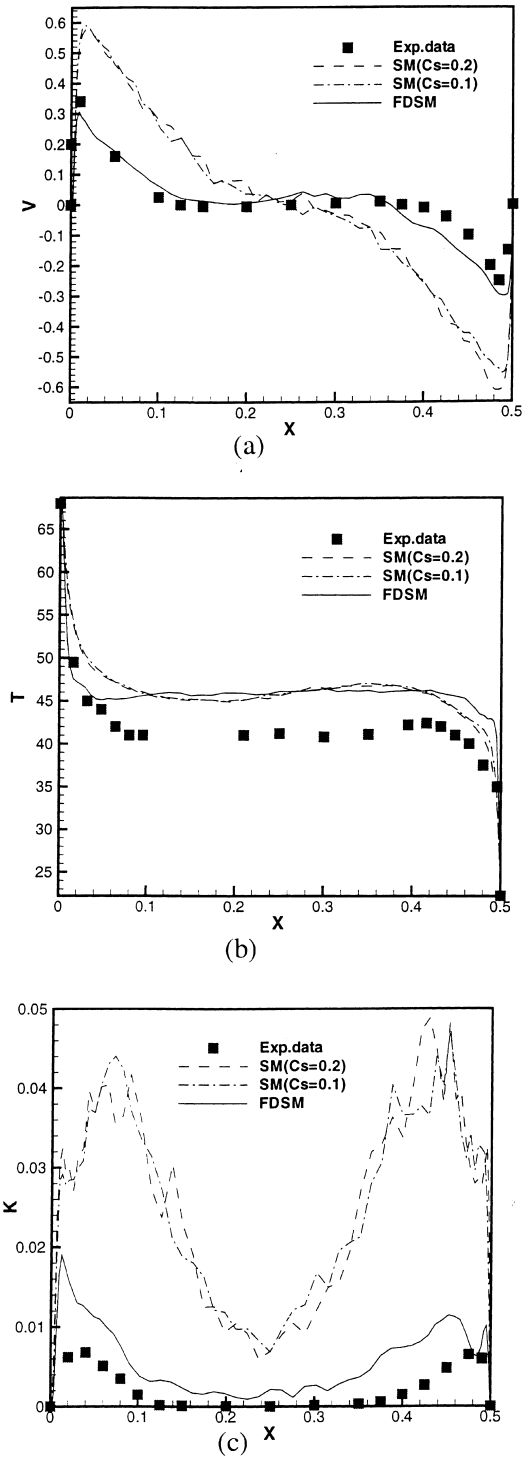

Fig. 2. Comparison of predicted and measured results at $y = AC/2$ section. (a) air velocity, (b) air temperature, and (c) turbulent energy.

forced, natural and mixed convections. For example, natural ventilation of a building is forced convection. Winter heating in a room by a baseboard heater is natural convection. Summer cooling in a room by an air-conditioner is mixed convection. In order to verify the ability of the FDSM model for all the three types of convection flows, the following sections show the results of LES simulations.

4.1. Natural convection

The investigation has selected the natural convection flow in a cavity as shown in Fig. 1(a). Cheesewright [22] has measured the air velocity, temperature, turbulent energy, and heat transfer in the cavity. Although the cavity is not the same as a room, the flow characteristics are similar to those in a room. The simple geometry eliminates many potential errors, such as those caused by the complex geometry of a baseboard heater. This would allow us to identify the reasons, if there are discrepancies between the computed results and measured data.

Since the natural convection consists of both turbulent and laminar flow, the flow is very challenging for the LES simulation. This study uses the SM ($C_S = 0.1$ and $C_S = 0.2$) and FDSM models to predict the distribution of air velocity, temperature, and turbulent intensity.

Fig. 1(a) shows the cavity geometry, height AC = 2.5 m, width AB = 0.5 m, and depth = 0.5 m. The temperature difference between warm and cold walls, $\Delta\theta$, was 45.8°C K (left wall temperature, θ_1, was 68.0°C, and right wall temperature, θ_2, was 22.2°C). All other walls were insulated. The flow corresponded to a Rayleigh number (Ra) of 5.0×10^{10}, where the Ra is defined as

$$Ra = \frac{(\theta_1 - \theta_2) g H^3}{\nu \alpha} \tag{34}$$

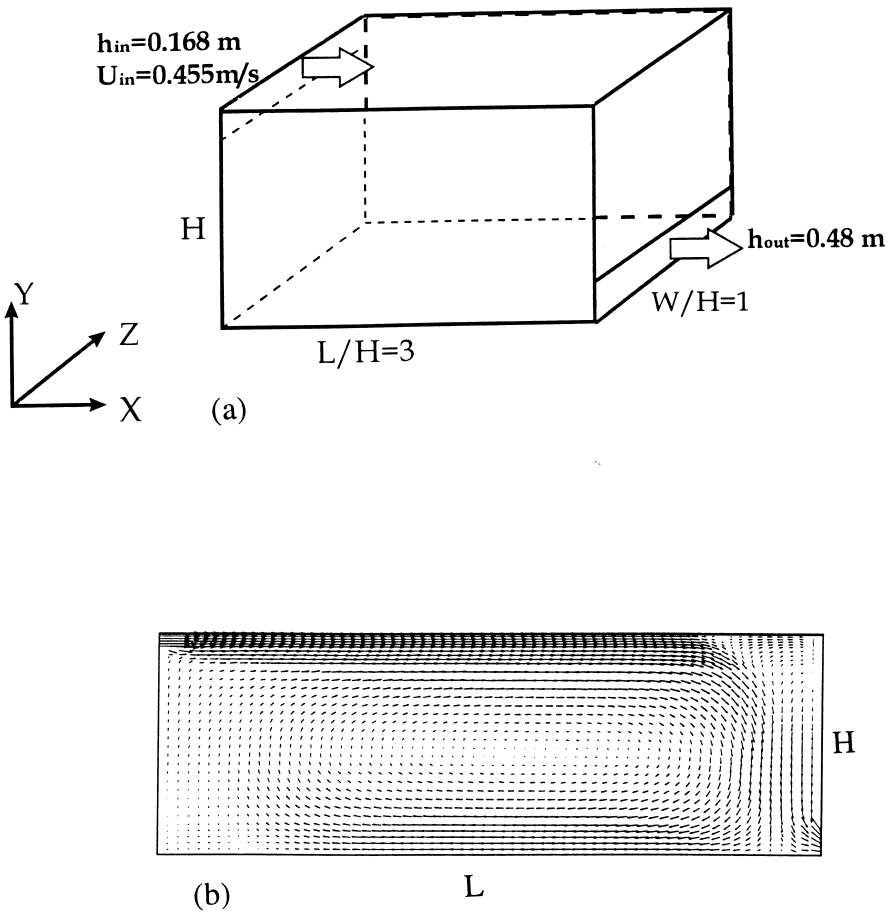

Fig. 3. The forced convection flow in a room. (a) room geometry and (b) average air velocity on the center plane by the FDSM.

The computations used no-slip velocity condition on all the walls. The meshes employed were $62 \times 62 \times 12$ for the height (x), width (y), and depth (z) directions, respectively. The time step $\Delta t = 0.0002$ s.

The computation used a zero initial air velocity and uniform 45.1°C air temperature for the whole flow domain. When the flow becomes statistically steady, the averaging technique is used to obtain the mean value of the computed parameters, such as average air velocity and temperature. The averaged time is about 120 s.

Fig. 1(b)–(d) show the distributions of the average air velocity, average air temperature, and instantaneous model coefficient C with FDSM at the center section (the depth is 0.25 m), respectively. The velocity field is asymmetric. The hot wall generates an upward flow near the wall and the cold wall a downward flow. The velocity in the center region of the cavity is generally small. The instantaneous C has a very large variation in the space. In the near wall and central region, the C approaches zero, where the flow is close to laminar.

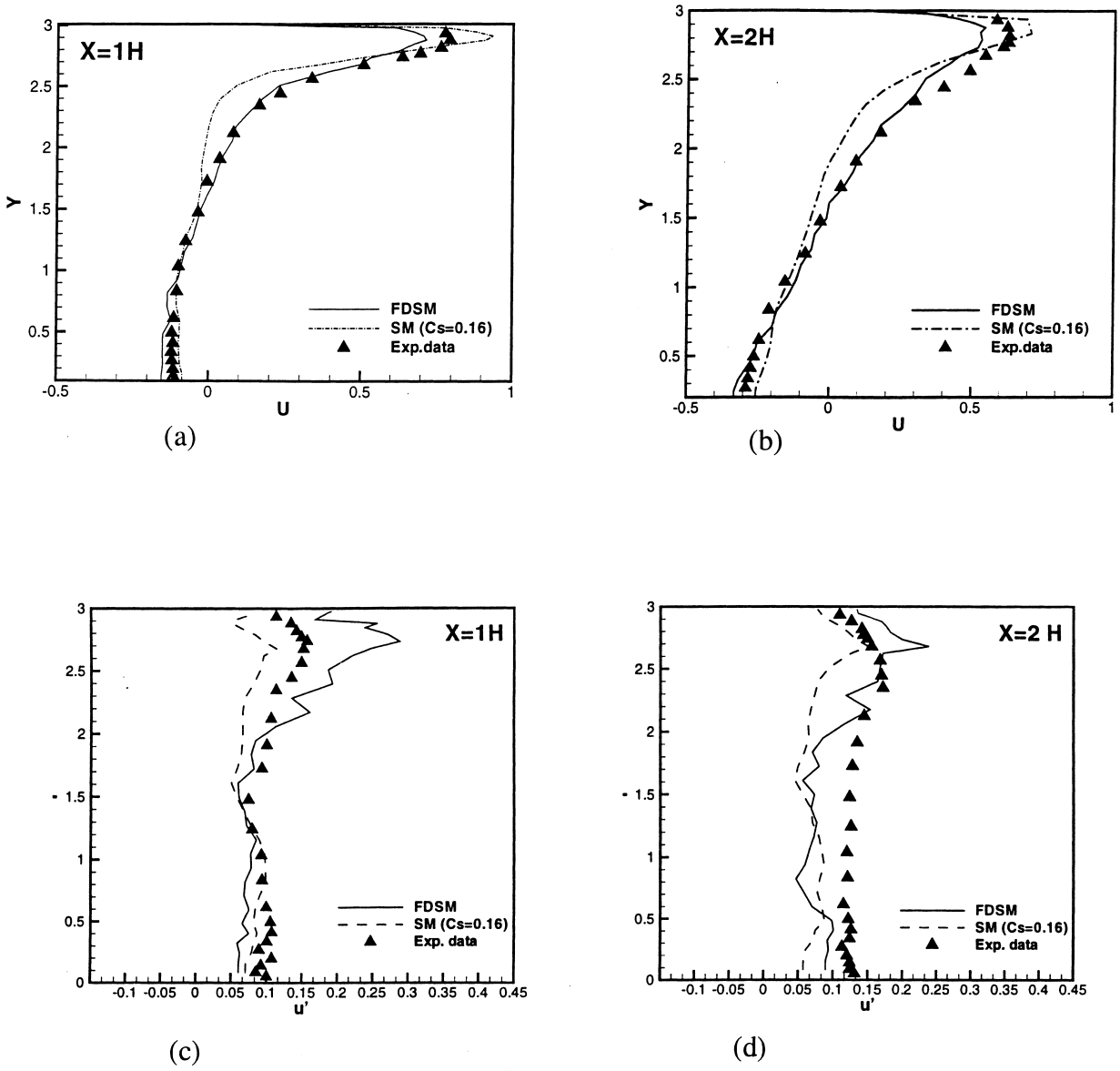

Fig. 4. Comparison of predicted and measured results on the center plane. (a) Average velocity profile at $x = 1H$, (b) average velocity profile at $x = 2H$, (c) velocity fluctuation profile at $x = 1H$, and (d) velocity fluctuation profile at $x = 2H$.

Fig. 2 compares the predicted and measured results in the cavity at $y = AC/2$. The performance of the SM with the two different coefficients was very poor. The SM model over-predicted the peak velocity near the walls by 85%, as shown in Fig. 2(a), compared with the experimental data. The main reason for the discrepancy is that the SM cannot predict the laminar flow near the wall and central region, although we have used the damping function for the near-wall laminar effect. The computed velocity profile with the FDSM agrees rather well with the experimental data. The FDSM is able to predict the flow structure as shown in the C distribution (Fig. 1(d)).

As reported by Cheesewright [22], the top and bottom walls were not well insulated in the experiment. The heat loss to the lab environment led to a lower mean air temperature in the cavity. As a result, the predicted mean air temperature in the cavity is higher than the measured data as illustrated in Fig. 2(b). All the computations have predicted a reasonable temperature distribution.

The paper calculates the turbulent energy as $\boldsymbol{k}=(u'^2 + v'^2 + w'^2)/2$. Fig. 2(c) compares the computed $\boldsymbol{k}$ profiles with the experimental data. The SM model over-predicted the turbulence energy by nearly 10 times. Since the SM used a constant C and turbulent energy is related to the C, the SM cannot predict correctly the turbulent energy profile. The performance of the FDSM is better than that of the SM, although it still over-predicts the turbulent energy, especially in the near wall region. As can be seen in Fig. 1(c), the C varies significantly in the near wall region.

4.2. Forced convection

For forced convection flow, the investigation used the case with experimental data from Nielsen [23]. The experiment used a scale model to simulate indoor airflow as shown in Fig. 3(a). The size of the model is $W/H = 1.0$, $L/H = 3.0$. The inlet height is $h_{in}/H = 0.056$, and outlet $h_{out}/H = 0.16$. The width of the inlet and outlet is the same as the model width. The flow Reynolds number was 5000, based on the inlet height. The computation used uniform air velocity profile at the inlet and zero gradient conditions at the outlet for air velocity. Simulations used the SM and FDSM. The SM is without the damping function, because the bulk Reynolds number was high. A wall function [24] was used for the walls. The wall function assumed the following instantaneous velocity profile near the walls:

$$\begin{array}{ll} u^+ = y^+ & \{y^+ < 11.6\} \\ u = 8.2y^{+1/7} & \{y^+ > 11.6\} \end{array}$$

The meshes employed were $46 \times 32 \times 16$ for the height (x), width (y), and depth (z) directions. The grid size is determined for an acceptable numerical accuracy with a reasonable computing time. The dimensionless time step $\Delta T (= \Delta t U_{in}/h_{in})$ is 0.002 in the calculations. In order to save CPU time, we used a k–ε model program to calculate this case with same grid first. Then, the LES simulation started from the results of a k–ε model prediction. When the calculation reaches statistically steady state, the averaging is performed over 800 dimensionless time. The calculation with the SM used 0.16 for the C_S, this C_S is a "better" value for indoor air prediction as tested by Murakami et al. [16].

Fig. 3(b) shows the averaged velocity distribution in the center section by the FDSM. The model can predict the re-circulation in the upper right corner. Chen [3] shows that none of the five k–ε models he tested was able to predict the re-circulation.

Fig. 4 compares the computed profiles of the vel-

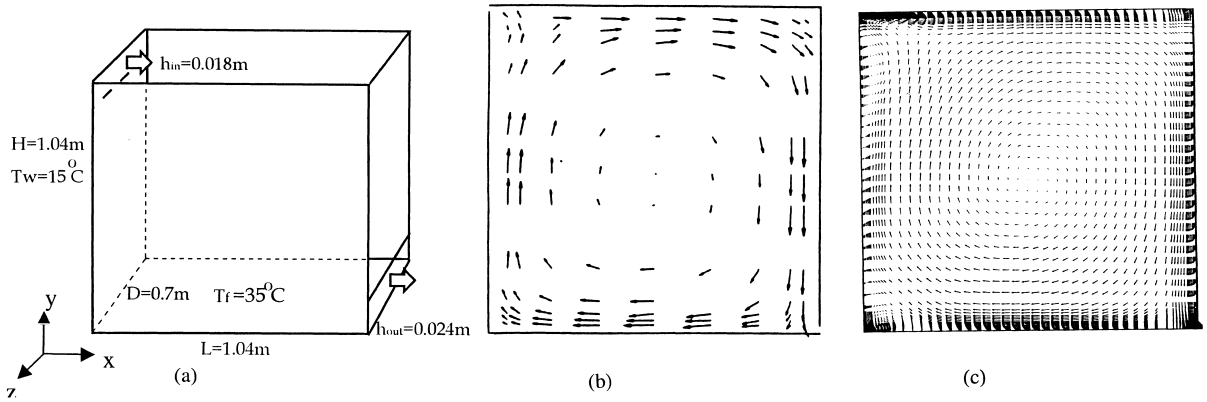

Fig. 5. The mixed convection flow in a room. (a) Room geometry, (b) average velocity vectors obtained from the experiment [23], and (c) average velocity vectors computed by the FDSM.

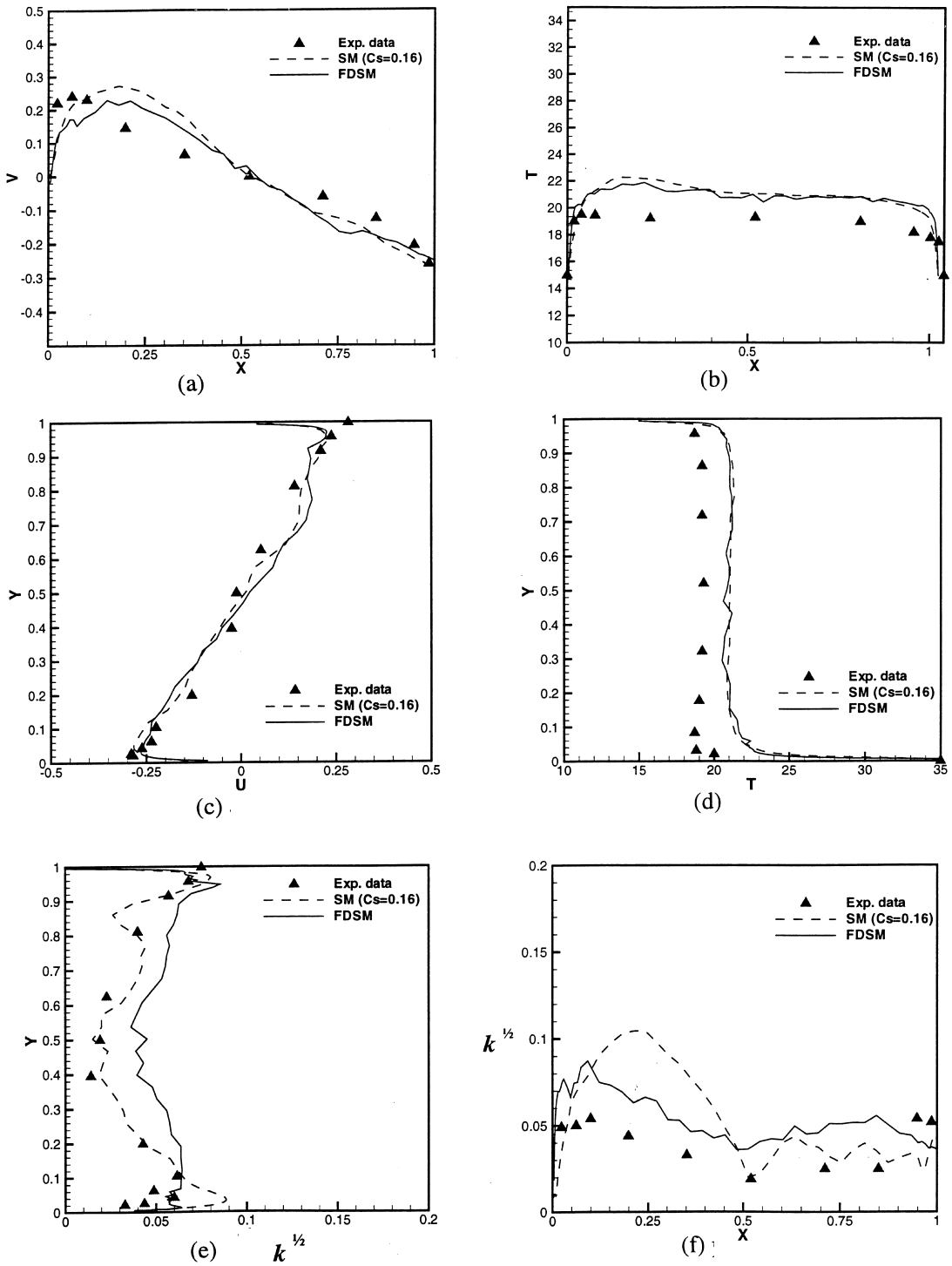

Fig. 6. Comparison of the predicted and measured results on the center sections. (a) Average velocity at $y = 0.502$ m, (b) average temperature at $y = 0.502$ m, (c) average velocity at $x = 0.502$ m, (d) average temperature at $x = 0.502$ m, (e) average turbulent energy ($k^{1/2}$) at $x = 0.502$ m, and (f) average turbulent energy ($k^{1/2}$) at $y = 0.502$ m.

ocity component in X direction, U, with the experimental data at $X = 1H$ (Fig. 4(a)) and $X = 2H$ (Fig. 4(b)), respectively. Again, the SM performs poorly for this case. The subgrid scale viscosity (ν_{SGS}) of the SM was under-predicted, and the models over-predicted the velocity at the jet region. On the other hand, the results with the FDSM agree well with the experimental data, except in the jet region. When the subgrid scale viscosity (ν_{SGS}) is over predicted, the velocity is smaller.

The problem of predicting the subgrid scale viscosity in the jet region is also reflected in the velocity fluctuation profile as shown in Fig. 4(c) and (d) for $X = 1H$ and $2H$ sections, respectively. The under-prediction of the subgrid scale viscosity in the jet region by the SM implies a lower turbulence level as shown in Fig. 4(c) and (d). In contrast, the over-prediction of the subgrid-scale viscosity in the jet region by the FDSM leads to a higher turbulence level. Furthermore, the coarse mesh distribution for the computations may also be attributed to the discrepancies.

4.3. Mixed convection

The present investigation used the case from Baly et al. [25] to study mixed convection flow in a room, as shown in Fig. 5(a). Baly et al. [25] measured air velocity, temperature, and turbulent energy for the case. The geometry of the test rig was $H = 1.04$ m long, $L = 1.04$ m wide, and $D = 0.7$ m deep. Again, this is a scale model of a room. The inlet height (h_{in}) was 0.018 m, the supply air velocity (U_{in}) 0.57 m/s, and supply air temperature (T_{in}) 15°C. The outlet height was 0.024 m. The model had a floor heating system that kept the floor temperature (T_f) to be 35°C. All other walls temperature (T_w) was 15°C. The corresponding Archimedes number, Ar ($Ar = \frac{\beta g h_{in} \Delta T_0}{U_{in}^2}$), is 0.0036 and Reynolds number, Re ($Re = \frac{U_{in} h_{in}}{\nu}$), is 678.

The computations used no-slip velocity condition on all the walls. The meshes employed were $62 \times 62 \times 12$ for the height (x), width (y), and depth (z) directions.

Fig. 5(c) shows the averaged air velocity distribution by the FDSM. Compared with the measured distribution (Fig. 5(b)), the airflow patterns are almost the same. The LES simulation shows a re-circulation in the left-bottom corner, but the re-circulation was not observed by the experiment. It is not clear if this is due to the insufficient fine measuring points or due to the model used.

Fig. 6 further compares the predicted mean air velocity, temperature, and turbulent energy by the SM ($C_S = 0.16$) and FDSM with the experimental data at two center sections at $Y = 0.35$ m. Fig. 6(a) and (b) show that the two subgrid scale models give very similar air velocity profiles. The predicted velocity profiles agree reasonably with the experimental data.

However, Fig. 6(c) and (d) indicate that the predicted air temperature is about 1.5 K higher than the measured one, although the shape of the predicted temperature profiles is the same as the measured one. Although the computations did not use a wall function for the solid boundaries, the models may over-predict the heat transfer from the floor or under-predict the heat transfer to the other walls. Since no detailed measurements on the heat transfer were available, it is difficult to identify the actual cause of the discrepancies. In addition, the Prandtl number of the subgrid scale may not be correctly modeled.

Fig. 6(e) and (f) illustrate that the computed turbulent energy profiles do not agree well with the experimental data. The performance of the FDSM model is slightly better than that of SM ($C_S = 0.16$).

5. Conclusions

The paper proposes a filtered dynamic subgrid scale model (FDSM) for the large eddy simulation of complex flow without a homogeneous direction, such as airflow with natural, forced, and mixed convection in a room. The computed results have been compared with those of the Smagorinsky model (SM) and the experimental data available from the literature.

The performance of the SM model for such flows was generally poor. It failed to predict even the mean flow parameters, such as mean air velocity and temperature. The model may over predict the turbulence level by one order.

The FDSM model can predict the airflow. The agreement between the computed results and the measured data is generally good. The model determines much better mean airflow parameters than turbulence parameters and heat transfer.

The results show that the large eddy simulation with the FDSM has a good potential to simulate indoor airflow.

Acknowledgements

The research was supported by the Center for Indoor Air Research. We would like to thank Prof. S. Murakami's group at the University of Tokyo for their useful suggestions.

References

[1] Q. Chen, Computational fluid dynamics for HVAC: successes and failures, ASHRAE Transactions 103 (1) (1997) 178–187.

[2] B.E. Launder, D.B. Spalding, The numerical compu-

tation of turbulent flows, Computer Methods in Applied Mechanics and Energy 3 (1974) 269–289.
[3] Q. Chen, Comparison of different k–ε models for indoor airflow computations, Numerical Heat Transfer (Part B: Fundamentals) 28 (1995) 353–369.
[4] Q. Chen, Prediction of room air motion by Reynolds-stress models, Building and Environment 31 (3) (1996) 233–244.
[5] J.W. Deardorff, A three dimensional numerical study of turbulent channel flow at large Reynolds numbers, J. Fluid Mechanics 41 (1970) 453.
[6] J. Smagorinsky, General circulation experiments with the primitive equations, I. The basic experiment, Monthly Weather Rev 91 (1963) 99–164.
[7] M. Germano, U. Piomelli, P. Moin, W.H. Cabot, A dynamic subgrid-scale eddy viscosity model, J. Physics Fluids A 3 (1991) 1760–1765.
[8] D.K. Lilly, A proposed modification of the Germano subgrid-scale closure method, J. Physics Fluids A 4 (1992) 633–635.
[9] M. Olsson, L. Fuchs, Large eddy simulation of proximal region of a spatially developing circular jet, J. Physics Fluids 8 (1996) 2125–2137.
[10] W. Rodi, J.H. Ferziger, M. Breuer, M. Pourquie, Status of large eddy simulation: results of a workshop, ASME J. Fluids Engineering 119 (1997) 248–262.
[11] Y. Zang, R.L. Street, J.R. Koseff, A dynamic mixed subgrid-scale model and its application to recalculating flow, J. Physics Fluid A 5 (1993) 3186–3195.
[12] S. Ghosal, T. Lund, P. Moin, K. Akselvoll, A dynamic localization model for large-eddy simulation of turbulent flows, J. Fluid Mechanics 286 (1995) 229–255.
[13] C. Meneveau, T. Lund, W.H. Cabot, A Lagrangian dynamic sub-grid scale model of turbulence, J. Fluid Mechanics 315 (1996) 353.
[14] P. Moin, Numerical and physical issues in large eddy simulation of turbulent flows, JSME International Journal B 41 (2) (1998) 454.
[15] L. Davidson, P. Nielsen, Large eddy simulation of the flow in a three-dimensional ventilated room, in: Proceedings of the Fifth International Conference on Air Distribution in Rooms, ROOMVENT'96, 1996, pp. 161–168.
[16] S.J. Emmerich, K.B. McGrattan, Application of a large eddy simulation model to study room airflow, ASHRAE Transactions 104 (1998).
[17] S. Murakami, A. Mochida, K. Matsui, Large eddy simulation of non-isothermal room airflow, comparison between standard and dynamic type of Smagorinsky model, SEISAN-KENKYU, Journal of Institute of Industrial Science, University of Tokyo 47 (2) (1995) 7–12.
[18] U. Piomelli, W.H. Cabot, P. Moin, S. Lee, Subgrid-scale backscatter in turbulent and transitional flows, J. Physics Fluids A 3 (1991) 1766.
[19] S. Ghosal, P. Moin, The basic equations for the large eddy simulation of turbulent flows in complex geometry, J. Computational Physics 118 (1995) 24–37.
[20] F.H. Harlow, J.E. Welch, Numerical calculation of time-dependent viscous incompressible flow, J. Physics Fluids 8 (1965) 12.
[21] H.L. Stone, Interactive solution of implicit approximations of multidimensional partial differential equations, SIAM J. Num. Anal 5 (1968) 530.
[22] R. Cheesewright, K.J. King, S. Ziai, Experimental data for the validation of computer codes for the prediction of two-dimensional buoyant cavity flows, in: ASME Winter Annual Meeting, Anaheim, December, HTD-60, 1986, p. 75.
[23] P.V. Nielsen, A. Restivo, J.H. Whitelaw, The velocity characteristics of ventilated room, ASME J. Fluids Engineering 100 (1978) 291–298.
[24] H. Wener, H. Wengla, Large eddy simulation of turbulent flow over and around a cube in plate channel, in: Proceedings of the Eighth Symposium on Turbulent Shear Flows, 1991, p. 155.
[25] D. Baly, S. Mergui, C. Niculae, Confined turbulent mixed convection in the presence of a horizontal buoyant wall jet, in: Fundamentals of Mixed Convection, HTD-Vol. 213, ASME, New York, 1992, pp. 65–72.